- 1 First observations of severe scintillation over low-to-mid latitudes driven by quiet-time
- 2 extreme equatorial plasma bubbles: conjugate measurements enabled by citizen science
- 3 initiatives
- 4 Sousasantos, J.<sup>1</sup>; Rodrigues, F. S.<sup>1</sup>; Gomez Socola, J.<sup>1</sup>; Pérez, C.; Colvero, F.<sup>2</sup>; Martinis, C. R.<sup>3</sup>;
- 5 and C. M. Wrasse<sup>4</sup>

- 7 Willian B. Hanson Center for Space Sciences, University of Texas at Dallas, Richardson, TX, USA
- 8 <sup>2</sup>Bate-Papo Astronômico Santa Maria Tecnoparque, Santa Maria, Rio Grande do Sul, Brazil
- <sup>3</sup>Center for Space Physics, Astronomy Department, Boston University, Boston, MA, USA
- <sup>4</sup>National Institute for Space Research, Space Weather Division, São José dos Campos, São Paulo, Brazil
- 11 Corresponding author: jonas.ssts@utdallas.edu

12

# 13 Keywords

- 14 Scintillation; extreme plasma bubbles; geomagnetic conjugate; geomagnetic quiet-time, citizen
- 15 science

16

17

#### Keypoints

- Citizen science initiatives allowed simultaneous observations of scintillation over geomagnetic conjugate areas at low-to-mid latitudes
- The observations show a conjugacy in the spatio-temporal evolution of intermediate scale size ionospheric irregularities
  - Low-to-mid latitude scintillations were associated with extreme EPBs (reaching dip latitudes > 26°) during geomagnetic quiet conditions

24

22

#### Abstract

Low-cost instrumentation combined with volunteering and citizen science educational initiatives allowed the deployment of L-band scintillation monitors to remote sense areas that are geomagnetically conjugated and located at low-to-mid latitudes in the American sector (Quebradillas in Puerto Rico and Santa Maria in Brazil). On October 10-11, 2023, both monitors detected severe scintillations, some reaching dip latitudes beyond 26°N. The observations show conjugacy in the spatio-temporal evolution of the scintillation-causing irregularities. With the aid of collocated all-sky airglow imager observations, it was shown that the observed scintillation event was caused by extreme Equatorial Plasma Bubbles (EPBs) reaching geomagnetic apex altitudes exceeding 2,200 km. The observations suggest that geomagnetic conjugate large-scale structures produced conditions for the development of intermediate scale (few 100s of meters) in both hemispheres, leading to scintillation at conjugate locations. Finally, unlike previous reports, it is shown that the extreme EPBs-driven scintillation reported here developed under geomagnetically quiet conditions.

### **Plain Summary**

The ionosphere is a region of the Earth's upper atmosphere characterized by a relatively large density of free ions and electrons produced, mainly, by solar photoionization. Ionospheric Equatorial Plasma Bubbles (EPBs) are drastic decreases in ionospheric density known to develop near the equator during nighttime and expand to low latitudes. EPBs cause fluctuations in transionospheric signals transmitted by Global Navigation Satellite Systems (GNSS) such as the GPS (Global Positioning System). In this report, we present the results of a study made possible by low-cost, GNSS-based sensors hosted by volunteers and citizen science educational initiatives. The study evaluated the behavior of scintillation in the northern and southern hemispheres at low-to-mid latitudes. We found similar spatio-temporal behavior in the scintillation events observed by monitors deployed in geomagnetically conjugate areas in the northern and southern hemispheres. We also found that the observed scintillation events were associated with EPBs that reached low-to-mid latitudes (extreme EPBs). Although these events are more likely to occur under disturbed geophysical conditions, the case presented here took place during a quiet period. The results indicate that GNSS systems at low-to-mid latitudes can be affected by EPBs-driven scintillation more often than previously anticipated.

#### Introduction

In recent years, there has been a growing number of reports describing the detection of events of ionospheric plasma depletions at low-to-mid and mid latitudes. These events have been connected to geomagnetic equatorial origins and can be classified into two categories. The first category is formed by Equatorial Plasma Bubbles (EPBs) reaching abnormally high geomagnetic apex altitudes (> 1500 km) and, therefore, dip latitudes in the low-to-mid latitude range (20°-30°). These events are referred to as super plasma bubbles (e.g., Ma and Maruyama, 2006; Cherniak and Zakharenkova, 2016) or extreme plasma bubbles (e.g., Cherniak and Zakharenkova, 2022; Sousasantos et al., 2023). The second category is formed by ionospheric plasma depletions reaching even higher geomagnetic apex altitudes (say 6,000 km or more) and more poleward dip latitudes (40° or more). Only a few of these events have been detected, and some of their behavior (e.g., zonal drift at mid latitudes) has been reported as not following the pattern expected for regular EPBs. This second category may involve a more complex connection between EPBs and high latitude plasma streams and are referred to as poleward-streaming plasma density depletions (Zhakharenkova and Cherniak, 2020; Cherniak and Zakharenkova, 2022).

The detection of low-to-mid and mid-latitude ionospheric plasma depletions was made possible, in great part, by observations made by increasing ground-based networks of instruments (e.g., geodetic Global Navigation Satellite System - GNSS receivers) and measurements covering wide areas that became available in recent years. The occurrence of extreme EPBs and poleward-streaming plasma density depletions is most often observed during geomagnetically disturbed periods (Basu et al., 2005; Basu et al., 2007; Ma and Maruyama, 2006; Huang et al., 2007; Martinis et al., 2015; Cherniak and Zakharenkova, 2016, 2022; Katamzi-Joseph et al., 2017; Aa et al., 2018, 2023; Li et al., 2018; Zakharenkova and Cherniak, 2020, 2021; Rodrigues et al., 2021; Sori et al., 2022; Sousasantos et al., 2023). Geomagnetic disturbances are known to affect the ionospheric electrodynamics and plasma structuring at low latitudes through the disturbance dynamo (Blanc and Richmond, 1980) and/or penetration electric fields (e.g., Senior and Blanc, 1984). The number of works evaluating the impacts of these events in terms of scintillation over low-to-mid latitudes, however, is way more limited.

Here, new results associated with the analyses of a comprehensive new set of observations of an event of extreme EPBs that drove severe scintillation at low-to-mid latitudes are reported. These new results include: (1) observations that were made in areas that are geomagnetically conjugate, allowing the track of the spatio-temporal evolution of scintillation-causing irregularities over corresponding geomagnetic field lines at both hemispheres; and (2) the evaluation of an event of extreme EPB-driven scintillation over low-to-mid latitudes (dip latitudes > 26°) during a geomagnetic quiet-time.

These observations were only possible due to advances in ground-based instrumentation and collaboration from volunteering and citizen science educational initiatives. In Quebradillas (Puerto Rico), one ground-based scintillation monitor was deployed at volunteer's house. In Santa Maria (Brazil), an identical monitor was deployed at the facility belonging to the Bate-Papo Astronômico-Santa Maria Tecnoparque, an initiative to promote and disseminate science for the general public in the areas of astronomy, astronautics and meteorology. More information (in Portuguese) can be found on their official webpage (<a href="https://batepapoastronomico.com/">https://batepapoastronomico.com/</a>).

The report is organized as follows: In Section 2, details about the instrumentation used in this study, their locations, and data sets are summarized. In Section 3, main results are presented and discussed. These results relate to: (a) the geomagnetic conditions under which the scintillation over low-to-mid latitudes were observed; (b) the spatio-temporal evolution of scintillation-causing irregularities over geomagnetic conjugate areas; (c) the relationship between the observed scintillation events and extreme EPBs. Finally, the main findings are summarized in Section 4.

## 2. Instruments, sites, and data sets

In this work, data from ScintPi 3.0 scintillation monitors were used to assess the severity of the amplitude scintillation and the latitudinal extent and apex altitudes of the scintillation-causing irregularities. ScintPi 3.0 can be described as low-cost, easy-to-install, and easy-to-maintain L-band ionospheric scintillation and Total Electron Content (TEC) monitor. It is based on Commercial Off-The-Shelf (COTS) dual-frequency GNSS receivers and Raspberry Pi single-board computers (Gomez Socola and Rodrigues, 2022).

Two ScintPi 3.0 monitors were deployed at locations that have geomagnetically conjugate areas in their fields-of-view (FOVs). One monitor was deployed in Quebradillas (Puerto Rico) and another in Santa Maria (Brazil). These monitors are hosted by a volunteer collaborator in Quebradillas and an educational center (Bate-Papo Astronômico-Santa Maria Tecnoparque) in Santa Maria. Data from October 10-11, 2023, when severe scintillations were detected over dip latitudes > 26°, were analyzed. The monitor in Quebradillas was deployed in December 2021 and the monitor in Santa Maria was deployed in June 2023.

The development, use, and performance of low-cost scintillation monitors have been reported in the literature (Rodrigues and Moraes, 2019; Vani et al., 2021; Freitas et al., 2022; Gomez Socola and Rodrigues, 2022). Low-cost monitors such as ScintPi provide an opportunity not only for research but for education as well (Wright et al., 2023). For instance, the system in Santa Maria is hosted by a citizen-led project ("Projeto Bate-Papo Astronomico") that promotes science with emphasis in the areas of astronomy, astronautics, and meteorology through observations and talks. ScintPi has helped with dissemination of information and engagement of learners in science. To reduce the work required from a host, ScintPi automatically acquire and upload the measurements to a server at The University of Texas at Dallas via internet. The hosts, however, have access to the server and can use the observations in their own initiatives.

The amplitude scintillation  $S_4$  index (Briggs and Parkin, 1963; Yeh and Liu, 1982) was used as a measure of scintillation severity. The  $S_4$  is defined as the standard deviation of the signal intensity normalized by the average intensity over an interval of 60s. Scintillation severity can be classified as weak  $(0.2 \le S_4 < 0.4)$ , moderate  $(0.4 \le S_4 < 0.7)$ , and severe  $(S_4 \ge 0.7)$  (e.g., Sreeja et al., 2020). The results used only data from satellites with elevation angles  $\ge 20^\circ$ . An exception was allowed for the results in Figure 4, where data from elevation angles  $\ge 10^\circ$  were used due to their relevance to the discussion.

To aid the interpretation of the scintillation measurements, observations of airglow (red line, 630.0 nm filter) made by all-sky imagers located in Culebra (Puerto Rico) and São Martinho da Serra (Brazil) were also analyzed. The all-sky imager in Culebra was moved from the Arecibo Observatory in 2023 and is part of the Boston University (BU) all-sky imager network (Martinis

et al., 2018) and is deployed at the Climate Center for Open Research and Education (CCORE). The imager in São Martinho da Serra is part of the Estudo e Monitoramento Brasileiro do Clima Espacial (EMBRACE) network at the Instituto Nacional de Pesquisas Espaciais (INPE), under a collaboration with the China-Brazil Joint Laboratory for Space Weather (CBJLSW). Information about the location of the ScintPi 3.0 monitors and all-sky imagers are provided in Table 1.

Station	Instrument	Geographic Longitude	Geographic Latitude	Dip Latitude (at 350 km)
Quebradillas	ScintPi 3.0	66.91°W	18.47°N	24.54°N
Culebra	All-sky imager	65.31°W	18.33°N	23.86°N
Santa Maria	ScintPi 3.0	53.87°W	29.68°S	22.19°S
São Martinho da Serra	All-sky imager	53.82°W	29.44°S	22.05°S

Table 1 – Identification of the stations and instruments, including the geographic coordinates and dip latitudes. The International Geomagnetic Reference Field 13 (IGRF-13) (Alken et al., 2021) was used to estimate the dip latitudes.

The geomagnetic indices Dst and Kp obtained at the NASA's Space Physics Data Facility repository and the Auroral Electrojet (AE) index (quicklook version) from the World Data Center for Geomagnetism, Kyoto University, were used to assess the geomagnetic conditions under which the observations were made.

#### 3. Results and Discussion

In this section, the results are detailed. First, the geomagnetic conditions during the event evaluated are presented, confirming that the extreme EPBs-driven scintillation over low-to-mid latitudes analyzed in this work occurred during a geomagnetically quiet period. In the sequence, the evolution of the scintillation over the conjugate areas is presented and discussed. Finally, airglow observations are used to confirm that the observed scintillation events were associated with extreme EPBs.

## 3.1. On the geomagnetic conditions during the extreme EPB of October 10-11, 2023

To assess the geomagnetic conditions during October 10-11, 2023, the geomagnetic indices Dst and Kp were used. Loewe and Prölss (1997) defined that a weak geomagnetic storm requires, in

general, at least  $Kp \ge 4$  and  $Dst \le -36$  nT (i.e., smaller values/absolute values of Kp/Dst indicate a quiet period). Figure 1 presents Dst (red line) and Kp (blue bars) values for October 7-12, showing that the magnitude of these geomagnetic indices remained at much lower levels, not only for the time of the observations but also during the four previous days.

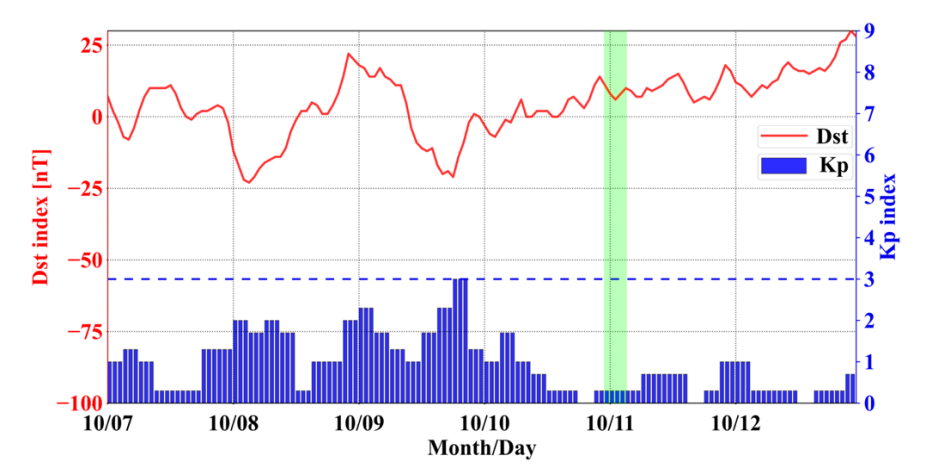


Figure 1 – Geomagnetic indices Dst (red) and Kp (blue) between October 7-12. The extreme EPBs-driven scintillations occurred in the night between October 10-11 (green shaded region). The blue dashed line highlights that Kp was always  $\leq$  3. Not only the hours when the scintillations occurred were under geomagnetically quiet conditions, but also the prior days.

The lowest values (largest "magnitudes") of Dst were -23 nT at 03:00UT on October 8 and -21 nT at 18:00UT on October 9. Kp reached at most 3.0 for 18:00-21:00 UT on October 9. Besides being considerably lower than the levels defined by Loewe and Prölss (1997), it must also be mentioned that these values occurred more than 24 hours prior to the observed scintillation. It is, then, unlikely that geomagnetic disturbances could have contributed to conditions favoring the development of extreme EPBs-driven scintillation at low-to-mid latitudes.

Finally, in addition to Dst and Kp, initial estimates of the Auroral Electrojet (AE) index were also analyzed to account for substorm contributions to the EPB event and the ensuing scintillation. So far, the provisional data is not available, but the "quicklook" version has already been posted at <a href="https://wdc.kugi.kyoto-u.ac.jp/ae\_realtime/index.html">https://wdc.kugi.kyoto-u.ac.jp/ae\_realtime/index.html</a>. AE values during October 10, 2023, were low with only a small and short increase (~300 nT) around 10:00 UT (i.e., more than 12 hours prior to the scintillation observed), and during October 11 the AE only had negligible values.

Therefore, it is also reasonable to assume that no contributions from substorms influenced the development of the extreme EPBs leading to scintillation.

## 3.2. On the spatio-temporal evolution of scintillations at geomagnetic conjugate regions

The monitors used in this study can make scintillation measurements using signals from multiple
GNSS constellations (Global Positioning System-GPS, Galileo, Beidou, and Globalnaya
Navigazionnaya Sputnikovaya Sistema - GLONASS). This feature allows a better tracking of the
spatio-temporal evolution of scintillation-causing irregularities within the field-of-view (FOV) of
the ground-based monitors. More importantly, the locations of the monitors in Quebradillas
(northern hemisphere) and Santa Maria (southern hemisphere) allow observing, simultaneously,
areas that are geomagnetically conjugate.

Several studies reported the geomagnetic conjugacy of large-scale (> 10s of km) ionospheric structures (e.g., Shiokawa et al., 2004, 2015; Martinis et al., 2007; Abdu et al., 2009; Sobral et al., 2009; Martinis et al., 2020). Conjugate observations of intermediate scale size (few 100s of meters) irregularities, however, have been extremely limited (e.g., de Paula et al, 2010; Sousasantos et al., 2022a). Theoretical works show that large-scale transverse polarization electric fields are expected to map efficiently along geomagnetic field lines (Farley et al., 1960). At smaller scales, however, the efficiency of electric field mapping is expected to be significantly reduced (Farley et al., 1960; Spreiter and Briggs, 1961; LaBelle, 1985). The observational setup and the event analyzed here allow for a case study of the behavior of low-to-mid latitude intermediate-scale irregularities causing L-band scintillation at geomagnetically conjugate locations.

To properly evaluate the geomagnetic conjugacy of scintillation as observed by these monitors, the measurements were analyzed according to Ionospheric Pierce Points – IPP (assumed to be at 350 km) for sequential time intervals, as shown in Figure 2. Recent works show that the altitude of the IPP must be chosen carefully to proper represent the situation. Closer to the dip equator, for instance, IPPs located at higher altitudes can be more well-suited (e.g., Espejo et al., 2022). The stations used in this work, however, are located at low-to-mid latitudes and both, simulations (Souza et al., 2020) and observations (Moro et al., 2022) indicate that, over these latitudes, the Fregion peak is commonly located around 350 km.

The scintillation values are for the L1  $\sim$  1.6 GHz signals and from all GNSS satellites and elevation angles greater than 20°.

The FOV of the Quebradillas (Santa Maria) ScintPi 3.0 monitor is represented by the region within the solid magenta (black) line. The region within the dashed magenta (black) line corresponds to the mapping of the FOV of Quebradillas (Santa Maria) to the conjugate hemisphere. The mapping was calculated using the International Geomagnetic Reference Field 13 (IGRF-13) (Alken et al., 2021).

Here, it is important to point out that the FOV of the Santa Maria monitor, mapped to the northern hemisphere (black dashed line), is mostly within the FOV of Quebradillas (magenta solid line). The same is not true for Quebradillas. That is, the mapping of the FOV of Quebradillas to the southern hemisphere (magenta dashed region) is not mostly within the FOV of Santa Maria. The distortion of the geomagnetic field lines causes the conjugate region of the FOV of Quebradillas monitor to cover a much wider area and reach more poleward latitudes in the southern hemisphere. Therefore, for the description and interpretation of the conjugate measurements the reader is recommended to focus on the Santa Maria measurements (FOV within the solid black line) and on conjugate observations in the northern hemisphere near Quebradillas (within the dashed black lines). For reference, isolines of dip latitudes (for 26°N and 26°S) are also shown in Figure 1. The dip latitudes were calculated using local magnetic coordinates obtained from the IGRF-13 (dip latitude=arctan[tan(magnetic inclination)/2]).

Figure 2 summarizes the conjugacy and spatio-temporal variation of scintillation-causing irregularities observed by the Santa Maria and Quebradillas monitors. First, Figure 2 (a) shows that no appreciable scintillation activity was observed by the Santa Maria and Quebradillas monitors on October 10 between 22:00 UT and 23:00 UT. Figure 2 (b), however, shows that the occurrence of moderate scintillation ( $S_4 > 0.4$ ) started to be observed in Santa Maria on October 10 between 23:00 UT and 24:00 UT. Scintillation occurrence also started in Quebradillas. More importantly, the scintillation in Quebradillas starts to be observed within the conjugate FOV

(within the dashed black line). In both cases, scintillation started to occur in the lower latitudes portion of the areas monitored by the sensors.

Figures 2 (c) and 2 (d) show that scintillation magnitudes increased in Santa Maria and extended to more poleward dip latitudes in the area within the FOV. The observations in Quebradillas within the conjugate area (i.e., within the dashed black line) also show a similar increase in the intensity of scintillation and an extension to more poleward dip latitudes. Figure 2 (e) might suggest that strong scintillation can be seen in Santa Maria without a counterpart in Quebradillas. This is because the location of severe scintillation observed by the Santa Maria monitor (indicated by the green arrow) maps to a conjugate region that had no measurements available (i.e., no corresponding IPPs observed over Quebradillas). The moderate scintillation observed in Santa Maria (indicated by the gray arrow), on the other hand, maps to a conjugate region where IPPs are available and confirm the occurrence of scintillation-causing irregularities on both hemispheres.

It must be emphasized here that the scintillation magnitudes are not expected to be the same in the observations over conjugate areas. The background densities that dictate the intensity of scintillation (de Paula et al., 2003; Rodrigues et al., 2021; Sousasantos et al., 2024a) in the two hemispheres are unlikely to be the same (Sousasantos et al., 2022a). Additionally, differences in the intensity of scintillations are expected since the distribution (e.g., elevation angles) of the IPPs in the two hemispheres are not the same and that can also influence the severity of the scintillation (Sousasantos et al., 2022b; Moraes et al., 2023). Finally, Figure 2 (f) shows that scintillation occurrence was negligible in both sites on October 11, between 03:00 and 04:00 UT.

In summary, the observations presented in Figure 2 show experimental evidence of similar spatiotemporal evolution of intermediate scale-size irregularities responsible for scintillation at geomagnetically conjugate areas. Given the low efficiency of the electric field mapping at those scales, one cannot expect that intermediate-scale irregularities are elongated from one hemisphere to the other. The observations would then indicate that the conjugate large-scale structures which do elongate, if any, could produce conditions that are favorable for the development of intermediate-scale irregularities in both hemispheres, at least for the event studied here.

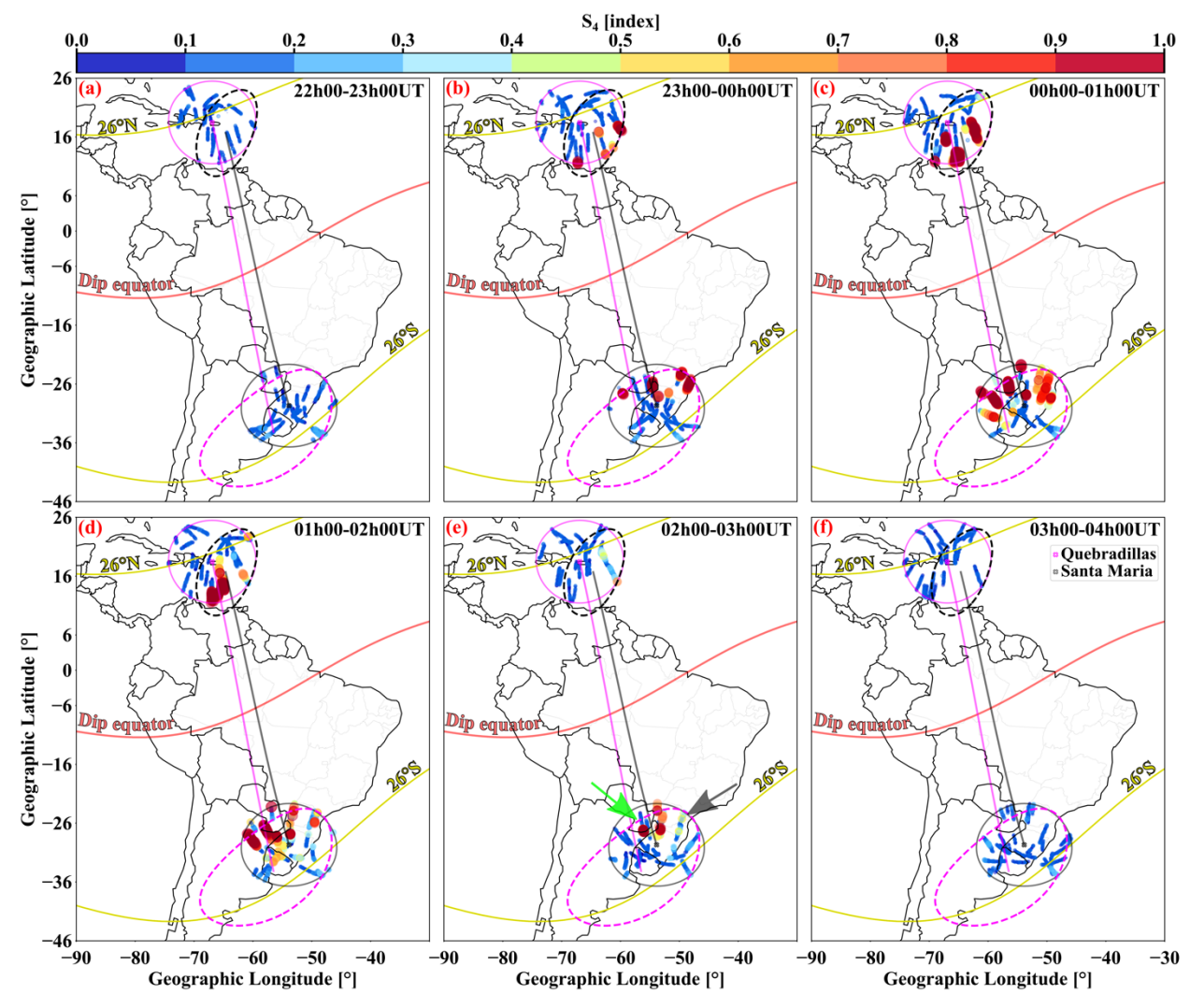


Figure 2 – Temporal evolution of amplitude scintillation over low-to-mid latitudes for conjugate stations in the northern and southern hemispheres. The values of the  $S_4$  index are indicated by the color bar at the top of the panels. The panels also show the FOVs of Quebradillas (magenta circle) and Santa Maria (black circle) and the projections of the conjugate regions corresponding to the FOVs of Quebradillas (magenta dashed region) in the southern hemisphere and Santa Maria (black dashed region) in the northern hemisphere. Isolines of dip latitudes at the equator (red) and  $\pm 26^{\circ}$  (yellow) are also depicted.

One additional statistical evaluation was performed (see Figure\_S2 in the supplementary material). For this analysis only the observations at Santa Maria (FOV within the solid black line) and the corresponding conjugate observations in the northern hemisphere near Quebradillas (within the dashed black lines) were used. Complementary Cumulative Distribution Functions (CCDFs) of S4 values were calculated hourly and show differences in the distribution of scintillation intensities observed at the two sites. This can be caused by several factors including differences in the plasma

drift conditions and background ionospheric densities (Sousasantos et al., 2022a), differences in the alignment of the signals with the geomagnetic field lines and differences in the geometry of the satellites (Sousasantos et al., 2022b).

### 3.3. The extreme EPB of October 10-11, 2023

The results summarized in Figure 2 and discussed in the previous section indicate a geomagnetic conjugate behavior of intermediate-scale size irregularities. It was then hypothesized that large-scale structures, if any, could map along magnetic field lines and create destabilizing conditions which would lead to intermediate-scale irregularities in the conjugate areas. In that case, the scintillation event of October 10-11, 2023, would have required, for instance, the occurrence of extreme EPBs reaching dip latitudes beyond 26° (i.e., magnetic apex altitudes higher than 2,200 km).

The timing and the spatial evolution of scintillation shown in Figure 2 indeed suggest that ionospheric irregularities were associated with EPBs. But, as mentioned earlier, the occurrence of EPBs reaching dip latitudes beyond 26° is unusual during geomagnetic quiet-time conditions, although hypothesized to be possible (e.g., Mendillo et al., 2005). Consequently, EPB-driven scintillation (and especially severe scintillation) is expected to be limited to smaller dip latitudes during geomagnetic quiet-time. Spogli et al. (2013) showed reasonable percentages of occurrence of  $S_4 > 0.25$  reaching regions up to dip latitudes of  $\sim 21.42^{\circ}$  (at that time), what is considerably smaller than 26°. Their work also did not separate occurrences during geomagnetic quiet and disturbed conditions and their percentages include all levels of scintillation, from weak (e.g., 0.2  $\leq$  S<sub>4</sub> < 0.4) up to possible severe cases (S<sub>4</sub>  $\geq$  0.7), not making distinction between quiet or disturbed events and weak or severe scintillation. More recently, Gomez Socola et al. (2023) analyzed three months of scintillation observations made by monitors in Puerto Rico and found that quiet-time scintillation was limited to dip latitudes smaller than 22°. On the other hand, Sousasantos et al. (2023) showed that, under geomagnetically disturbed conditions, extreme EPBs-driven scintillation can develop and reach dip latitudes beyond 28°. Therefore, attributing the scintillation event to extreme EPBs would benefit from additional experimental evidence.

Additional evidence that the scintillation event of October 10-11, 2023, was indeed associated with extreme EPBs and large-scale plasma structuring in conjugate areas comes from all-sky airglow imagers installed in Culebra (Puerto Rico) and São Martinho da Serra (Brazil). The airglow measurements made by the São Martinho da Serra and Culebra imagers cover the FOVs of Santa Maria and Quebradillas ScintPis, respectively.

Figure 3 summarizes the analyses of the collocated airglow and scintillation observations. The upper panels show a sequence of unwarped airglow images observed by the Culebra imager between October 10, 23:30 UT and October 11, 01:30 UT. The lower panels show airglow images from São Martinho da Serra for the same period. Over both locations, the images were unwarped, considering altitudes of 250 km. The images show the dark streaks that are commonly associated with EPB depletions. As expected from the behavior of EPBs, the depletions are first observed at low dip latitudes and extend poleward with time. Features such as bifurcations, which are also common signatures of EPBs can also be seen in the images. The images serve to confirm the occurrence of extreme EPBs reaching dip latitudes beyond 26° N (apex altitudes above 2,200 km).

In addition to airglow images, Figure 3 also shows IPPs and observed  $S_4$  values. The  $S_4$  values are for  $\pm 30$ -minute intervals around the time of the airglow observations ( $\sim 23:30$  UT,  $\sim 00:30$  UT,  $\sim 01:30$  UT, from left to right, respectively). The  $S_4$  values are represented by the color bar above the panels. The dashed white line in the Culebra images represents the geomagnetic region that is conjugate of the Santa Maria ScintPi FOV.

Figure 3 shows an excellent agreement between the locations of scintillation occurrence and the EPBs, despite uncertainties in the altitude of the irregularities causing scintillation. The IPPs were computed assuming a mean altitude of 350 km. The airglow images also confirm the conjugacy of the EPBs structures. For instance, three different EPB structures labelled A, B, and C are indicated in the panels showing the images at ~01:30 UT (right-hand side of Figure 2) and can be identified in the airglow observations over both hemispheres. It is important to recall that this is a geomagnetically quiet-time event.

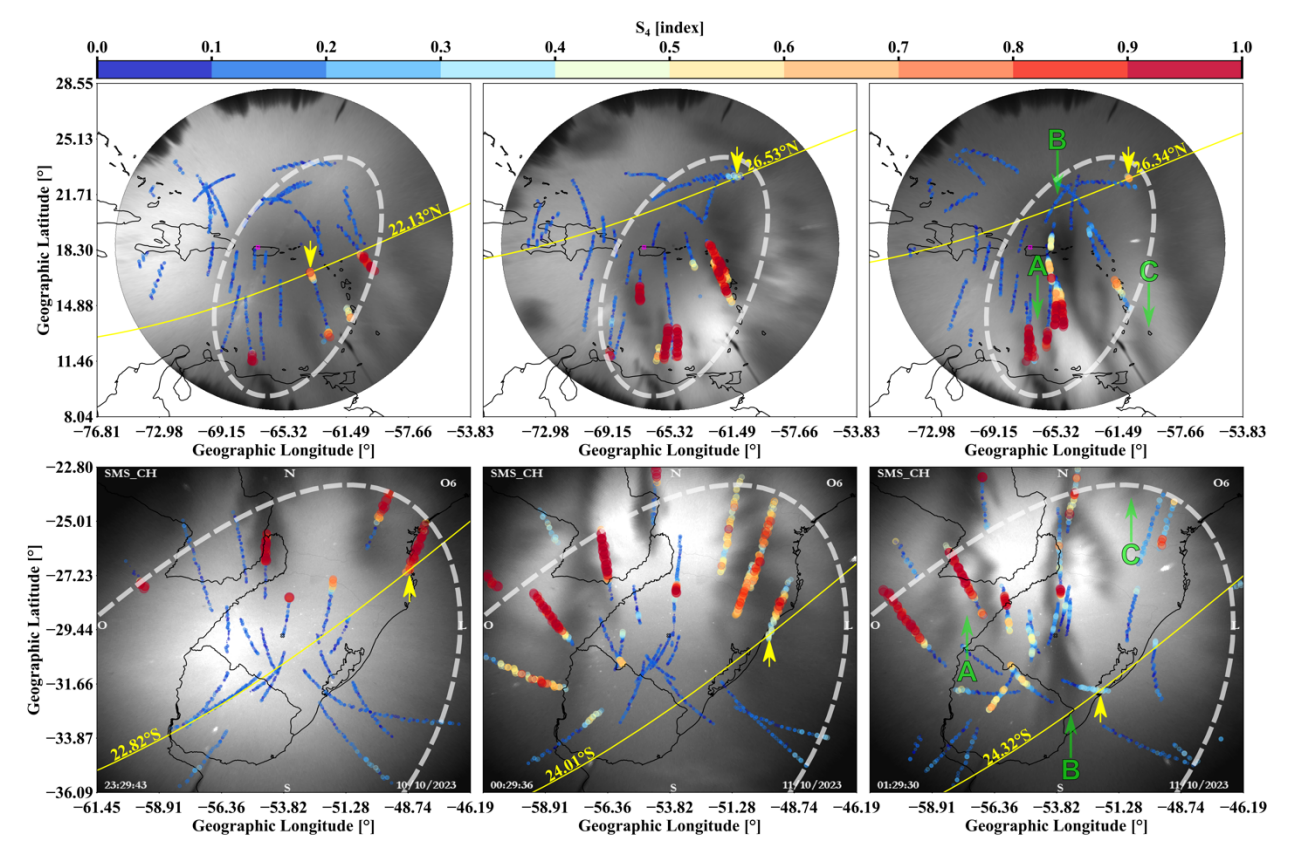


Figure 3 – All-sky images over Quebradillas (upper panels) and Santa Maria (lower panels) and the amplitude scintillation index S<sub>4</sub> (colors) for three different times (~23:30 UT, ~00:30 UT, and ~01:30 UT). The conjugate region of the FOVs of the ground-based scintillation monitors at Quebradillas/Santa Maria over the opposite hemisphere (white dashed lines) are also depicted. For reference, yellow arrows and isolines indicate, respectively, some locations of moderate and severe scintillation and dip latitudes.

To provide a clearer perspective of the reach of these quiet-time extreme EPBs and the associated ionospheric scintillation over low-to-mid latitudes, Figure 4 was prepared. It shows the collocated observations over the northern hemisphere. Unlike all the previous analyses, here the elevation angle constraint was decreased to  $\geq 10^{\circ}$  to cover regions more to the east, closer to the longitudinal limits of the all-sky coverage. The resulting FOV of the ScintPi is depicted in Figure 4. In this figure, the S<sub>4</sub> values correspond to the L2 frequency ( $\sim 1.2$  GHz). The all-sky image is for  $\sim 01:30$  UT, and the S<sub>4</sub> values are for the  $\pm 30$ -minute interval around the image hour.

From Figure 4 it is evident that: (1) the "scintillation patch" appearing in the eastern part of the field of view is associated with the quiet-time extreme EPB indicated by the yellow arrow; and (2) the scintillation patch reached dip latitudes beyond 26°N and values of  $S_4 = 0.9$ . In summary,

unlike conventionally thought, the results presented here demonstrate that extreme-EPB driven severe scintillation can occur over low-to-mid latitudes also under geomagnetically quiet conditions.

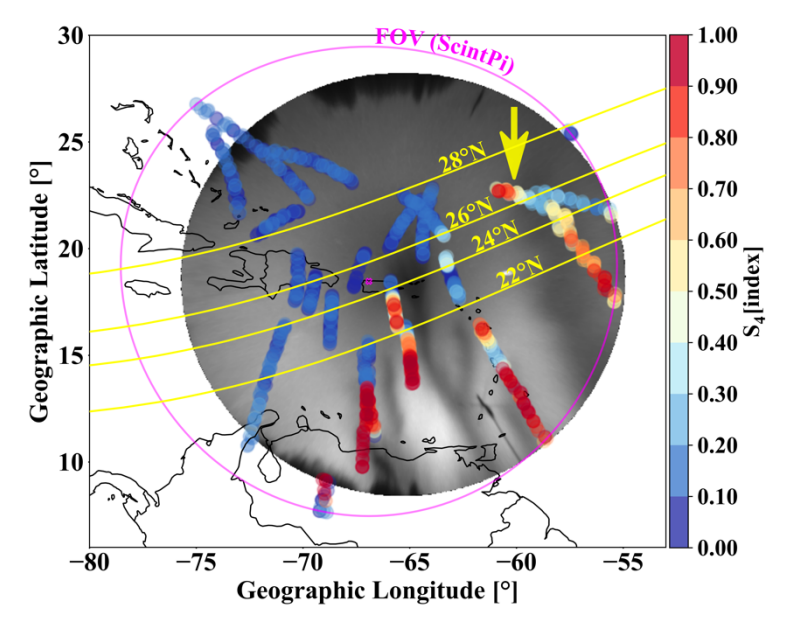


Figure 4 – Combined observation of extreme EPBs and associated severe scintillation under geomagnetic quiet-time over low-to-mid latitudes in the northern hemisphere. The "scintillation patch" highlighted by the yellow arrow clearly reaches dip latitudes beyond  $26^{\circ}N$  and values of  $S_4 = 0.9$ .

It may be mentioned here that another event was observed by the scintillation monitors on November 02-03 (Figure\_S1 in the supplementary material) with  $S_4$  (L1) reaching  $\sim 0.6$  at dip latitudes of 25.47°N (geographic coordinates: 63.68°W, 20.75°N), corresponding to an apex altitude of  $\sim$ 2021 km. Inspection of the Culebra all-sky images confirmed that the scintillation was also caused by quiet-time extreme EPBs. The airglow images can be accessed at <a href="http://sirius.bu.edu/dataview/?location=culebra&year=2023&filt=6300&month=Nov&day=3">http://sirius.bu.edu/dataview/?location=culebra&year=2023&filt=6300&month=Nov&day=3</a>.

It is possible that the lack of routine observations at low-to-mid latitudes might have led to the idea that severe scintillation over low-to-mid latitudes would only occur during geomagnetic disturbed conditions or that events other than EPBs would be related to the occurrence of severe scintillation over low-to-mid latitudes. But as the solar cycle 25 rises, an increase in the occurrence of extreme EPBs is expected. As a result, intense scintillation at low-to-mid latitudes during both, geomagnetically quiet and disturbed periods, may occur. Scintillation measurements such as those presented here and supported by our citizen science collaborators can contribute to a better

understanding of how events of equatorial origin, such as EPBs, can reach the low-to-mid latitudes and impact GNSS operations under distinct geophysical conditions.

This study provides the first observations showing that severe scintillation can be experienced over dip latitudes > 26° during geomagnetically quiet conditions. The underlying physical conditions favoring the development of quiet-time extreme EPBs remain to be investigated and discussed in a future work, when complementary thermospheric and ionospheric observations are available. It must be point out, however, that Mendillo et al. (2005) hypothesized that the altitude/latitude extent of the EPBs is controlled by the flux tube integrated ion mass density. More specifically, that EPBs would stop rising when the magnetic flux-tube-integrated ion mass density inside the EPB equals that of the surrounding background ionosphere (Krall et al., 2010). Therefore, the EPB observations might indicate that larger than usual scale lengths of the integrated ion mass density height profiles can occur even during geomagnetic quiet conditions caused, perhaps, by the quiet-time variability of low latitude F-region drifts or of the ionospheric plasma density latitudinal distribution.

### 4. Conclusions

Two ScintPi 3.0 scintillation monitors were deployed at sites located at low-to-mid latitudes in the northern and southern hemispheres with the aid of volunteering and citizen science educational collaborators. These monitors allowed simultaneous observations of scintillation and the evaluation of its spatio-temporal evolution over geomagnetic conjugate areas in the American sector.

This work reports observations made on October 10-11, 2023, that provide experimental evidence of similar behavior of intermediate-scale (a few 100s of meters) irregularities causing L-band scintillation at geomagnetically conjugate areas. While scintillation-causing irregularities are not expected to elongate from one hemisphere to another, it is suggested here that large-scale ionospheric structures that can map along field lines could produce conditions favoring the development of intermediate-scale irregularities and L-band scintillation in both hemispheres.

Additionally, since scintillation observed by the monitors reached dip latitudes beyond 26°, this event would require the occurrence of extreme EPBs capable of attaining apex altitudes above 2,200 km over the geomagnetic equator. Simultaneous and collocated measurements made by all-sky airglow imagers were used to confirm that the scintillations were indeed associated with quiet-time extreme EPBs. The images also confirmed that similar large-scale perturbations occurred in the conjugate areas, providing conditions for similar behavior in scintillation-causing irregularities.

The observations also show that, unlike events presented in previous studies that focused on geomagnetically disturbed conditions, extreme EPBs and severe scintillation can reach dip latitudes above 26° under geomagnetically quiet conditions. Routine (uninterrupted) scintillation observations in Quebradillas and Santa Maria can contribute to a better understanding about how far, in dip latitude or apex height, can EPBs extend under different conditions of geomagnetic and solar activity. It is possible that scintillation effects associated with EPBs can affect GNSS systems located in the low-to-mid latitude region more often than previously anticipated.

77/

## Acknowledgments

460

- Work at UT Dallas is supported by NSF Awards AGS-2122639, AGS-1916055. The Climate
- 462 Center for Open Research and Education (CCORE) is supported by the Florida Space Institute
- 463 (FSI)/University of Central Florida (UCF), and by the NSF Award AGS Grant-2221770.
- 464 CM acknowledges the support of NSF Aeronomy grant AGS-2152365 and NASA grant
- 465 80NSSC22K0095. CM acknowledges the support of P. Terra and C. Brum (funded by NSF Award
- 466 AGS-2221770) and Personnel of Climate Center for Open Research and Education (CCORE) at
- 467 Culebra, Puerto Rico, for operation of the BU all-sky imager. Quick-look images and moves can
- be found at www.buimaging.com.
- 469 CM Wrasse was supported by Conselho Nacional de Desenvolvimento Científico e Tecnológico
- 470 (CNPQ) under grant number 313911/2023-1 and thanks also to The China-Brazil Joint Laboratory
- 471 for Space Weather (CBJLSW) of the National Space Science Center (NSSC) at the Chinese
- 472 Academy of Science (CAS), grant numbers 183311KYSB20200003 and 183311KYSB20200017,
- 473 for supporting the all-sky imager data at São Martinho da Serra (Brazil). The data were available
- at INPE/EMBRACE website <a href="https://www2.inpe.br/climaespacial/portal/linear-image-video/">https://www2.inpe.br/climaespacial/portal/linear-image-video/</a>.
- The authors also acknowledge Ariane Silva Jardim and Diogo Machado Custodio who also work
- in the Bate-Papo Astronômico Santa Maria Tecnoparque initiative.
- 477 Authors would like to thank the International Association of Geomagnetism and Aeronomy
- 478 (IAGA) and all the scientific and technical staff responsible for the distribution of the International
- 479 Geomagnetic Reference Field (IGRF). The authors acknowledge the NASA Space Physics Data
- 480 Facility staff.

481 482

483

### **Data Availability Statement**

- 484 The all-sky data from Culebra and São Martinho da Serra can be accessed at
- http://sirius.bu.edu/dataview/ and https://www2.inpe.br/climaespacial/portal/linear-image-video/,
- respectively. IGRF13 can be accessed at https://www.ngdc.noaa.gov/IAGA/vmod/igrf.html. The
- Dst and Kp indices can be accessed at <a href="https://omniweb.gsfc.nasa.gov/form/dx1.html">https://omniweb.gsfc.nasa.gov/form/dx1.html</a>. AE index
- 488 (Quicklook) is available at <a href="https://wdc.kugi.kyoto-u.ac.jp/ae-realtime/index.html">https://wdc.kugi.kyoto-u.ac.jp/ae-realtime/index.html</a>.
- 489 ScintPi data used is available at (Sousasantos et al., 2024 b).

#### 491 References

- 492 Aa, E.; Huang, W.; Liu, S.; Ridley, A.; Zou, S.; Shi, L.; Chen, Y.; Shen, H.; Yuan, T.; Li, J.; and T.
- Wang (2018). Midlatitude plasma bubbles over China and adjacent areas during a magnetic storm
- on 8 September 2017. Space Weather, v. 16 (3), p. 321-331, doi: 10.1002/2017SW001776.

495

- 496 Aa, E.; Zhang, S. R.; Erickson, P. J.; Wang, W.; Qian, L.; Cai, X.; Coster, A. J.; and L. P.
- 497 Goncharenko (2023). Significant mid- and low-latitude ionospheric disturbances characterized by
- 498 dynamic EIA, EPBs, and SED variations during the 13–14 March 2022 geomagnetic storm.
- 499 Journal of Geophysical Research: Space Physics, v. 128 (8), p. 1-23, doi: 10.1029/2023JA031375.

500

- Abdu, M. A.; Batista, I. S.; Reinisch, B. W.; de Souza, J. R.; Sobral, J. H. A.; Pedersen, T. R.;
- Medeiros, A. F.; Schuch, N. J.; de Paula, E. R.; and K. M. Groves (2009). Conjugate Point
- 503 Equatorial Experiment (COPEX) campaign in Brazil: Electrodynamics highlights on spread F
- 504 development conditions and day-to-day variability. Journal of Geophysical Research: Space
- 505 Physics, v. 114 (A4), p. 1-21, doi: 10.1029/2008JA013749.

506

- Alken, P.; Thébault, E.; Beggan, C. D.; Amit, H.; Aubert, J.; Baerenzung, J.; Bondar, T. N.; Brown,
- W. J.; Califf, S.; Chambodut, A.; Chulliat, A.; Cox, G. A.; Finlay, C. C.; Fournier, A.; Gillet, N.;
- Grayver, A.; Hammer, M. D.; Holschneider, M.; Huder, L.; Hulot, G.; Jager, T.; Kloss, C.; Korte,
- M.; Kuang, W.; Kuvshinov, A.; Langlais, B.; Léger, J. M.; Lesur, V.; Livermore, P. W.; Lowes, F.
- J.; Macmillan, S.; Magnes, W.; Mandea, M.; Marsal, S.; Matzka, J.; Metman, M. C.; Minami, T.;
- Morschhauser, A.; Mound, J. E.; Nair, M.; Nakano, S.; Olsen, N.; Pavón-Carrasco, F. J.; Petrov, V.
- G.; Ropp, G.; Rother, M.; Sabaka, T. J.; Sanchez, S.; Saturnino, D.; Schnepf, N. R.; Shen, X.;
- 514 Stolle, C.; Tangborn, A.; Tøffner-Clausen, L.; Toh, H.; Torta, J. M.; Varner, J.; Vervelidou, F.;
- Vigneron, P.; Wardinski, I.; Wicht, J.; Woods, A.; Yang, Y.; Zeren, Z.; and B. Zhou (2021).
- International Geomagnetic Reference Field: the thirteenth generation. Earth, Planets and Space, v.
- 517 73 (49), p. 1-25, doi: 10.1186/s40623-020-01288-x.

- Basu, S.; Basu, S.; Groves, K. M.; MacKenzie, E.; Keskinen, M. J.; and F. J. Rich (2005). Near-
- 520 simultaneous plasma structuring in the midlatitude and equatorial ionosphere during magnetic
- 521 superstorms. Geophysical Research Letters, v. 32 (12), p. 1-4, doi: 10.1029/2004GL021678.

- Basu, S.; Basu, S.; Rich, F. J.; Groves, K. M.; MacKenzie, E.; Coker, C.; Sahai, Y.; Fagundes, P.
- R.; and F. B. Guedes (2007). Response of the equatorial ionosphere at dusk to penetration electric
- fields during intense magnetic storms. Journal of Geophysical Research: Space Physics, v. 112
- 526 (A8), p. 1-14, doi: 10.1029/2006JA012192.

527

- 528 Blanc, M.; and A. D. Richmond (1980). The ionospheric disturbance dynamo. Journal of
- Geophysical Research: Space Physics, v. 85 (A4), p. 1669-1686, doi: 10.1029/JA085IA04P01669.

530

- Briggs, B. H.; and I. A. Parkin (1963). On the variation of radio star and satellite scintillations with
- zenith angle. Journal of Atmospheric and Terrestrial Physics, v. 25 (6), p. 339-366, doi:
- 533 10.1016/0021-9169(63)90150-8.

534

- Cherniak, I.; and I. Zakharenkova (2016). First observations of super plasma bubbles in Europe.
- 536 Geophysical Research Letters, v. 43 (21), p. 11137-11145, doi: 10.1002/2016GL071421.

537

- 538 Cherniak, I.; and I. Zakharenkova (2022). Development of the storm-induced ionospheric
- 539 irregularities at equatorial and middle latitudes during the 25-26 august 2018 geomagnetic storm.
- 540 Space Weather, v. 20 (2), p. 1-18, doi: 10.1029/2021SW002891.

541

- de Paula, E. R.; Rodrigues, F. S.; Iyer, K. N.; Kantor, I. J.; Abdu, M. A.; Kintner, P. M.; Ledvina,
- B. M.; and H. Kil (2003). Equatorial anomaly effects on GPS scintillations in Brazil. Advances in
- 544 Space Research, v. 31(3), p. 749–754, doi: 10.1016/S0273-1177(03)00048-6.

545

- de Paula, E. R.; Muella, M. T. A. H.; Sobral, J. H. A.; Abdu, M. A.; Batista, I. S.; Beach, T. L.; and
- 547 K. M. Groves (2010). Magnetic conjugate point observations of kilometer and hundred-meter scale
- 548 irregularities and zonal drifts. Journal of Geophysical Research: Space Physics, v. 115 (A8), p. 1-
- 549 15, doi: 10.1029/2010JA015383.

- Eastes, R. W.; McClintock, W. E.; Burns, A. G.; Anderson, D. N.; Andersson, L.; Codrescu, M.;
- 552 Correira, J. T.; Daniell, R. E.; England, S. L.; Evans, J. S.; Harvey, J.; Krywonos, A.; Lumpe, J.

- D.; Richmond, A. D.; Rusch, D. W.; Siegmund, O.; Solomon, S. C.; Strickland, D. J.; Woods, T.
- N.; Aksnes, A.; Budzien, S. A.; Dymond, K. F.; Eparvier, F. G.; Martinis, C. R.; and J. Oberheide
- 555 (2017). The Global-scale Observations of the Limb and Disk (GOLD) mission. Space Science
- 556 Reviews, v. 212 p. 383-408, doi: 10.1007/s11214-017-0392-2.

- Espejo, T. M. S.; Costa, E.; de Paula, E. R.; Moraes, A. O.; and J. F. G. Monico (2022). Variability
- of Vertical Total Electron Content Gradients in the Brazilian Sector. IEEE Transactions on
- 560 Aerospace and Electronic Systems, v. 59 (3), p. 2687-2701, doi: 10.1109/TAES.2022.3218520.

561

- Farley, D. T. (1960). A theory of electrostatic fields in the ionosphere at nonpolar geomagnetic
- 563 latitudes. Journal of Geophysical Research, v. 65 (3), p. 1225-1233, doi:
- 564 10.1029/JZ065i003p00869.

565

- Freitas, M. J. S.; Moraes, A. O.; Marques, J. C.; and F. S. Rodrigues (2022). A contribution to real-
- 567 time space weather monitoring based on scintillation observations and IoT. Advances in Space
- 568 Research, v. 70 (2), p. 456-469, doi:10.1016/j.asr.2022.04.058.

569

- Gomez Socola, J.; and F. S. Rodrigues (2022). ScintPi 2.0 and 3.0: low-cost GNSS-based monitors
- of ionospheric scintillation and total electron content. Earth, Planets and Space, v. 74 (185), p. 1-
- 572 18, doi: 10.1186/s40623-022-01743-x.

573

- Gomez Socola, J.; Sousasantos, J.; Rodrigues, F. S.; Brum, C. G. M.; Terra, P.; Moraes, A. O.; and
- R. W. Eastes (2023). On the quiet-time occurrence rates, severity and origin of L-band ionospheric
- 576 scintillations observed from low-to-mid latitude sites located in Puerto Rico. Journal of
- 577 Atmospheric and Solar-Terrestrial Physics, v. 250, p. 1-9, doi: 10.1016/j.jastp.2023.106123.

578

- Huang, C. S.; Foster, J. C.; and Y. Sahai (2007). Significant depletions of the ionospheric plasma
- 580 density at middle latitudes: A possible signature of equatorial spread F bubbles near the
- plasmapause. Journal of Geophysical Research: Space Physics, v. 112 (A5), p. 1-13, doi:
- 582 10.1029/2007JA012307.

- Katamzi-Joseph, Z. T.; Habarulema, J. B.; and M. Hernández-Pajares (2017). Midlatitude
- postsunset plasma bubbles observed over Europe during intense storms in April 2000 and 2001.
- 586 Space Weather, v. 15 (9), p. 1177-1190, doi: 10.1002/2017SW001674.

- Krall, J.; Huba, J. D.; Ossakow, S. L.; and G Joyce (2010). Why do equatorial ionospheric bubbles
- stop rising? Geophysical Research Letters, v. 37 (9), p. 1-4, doi: 10.1029/2010GL043128.

590

- J. LaBelle (1985). Mapping of electric field structures from the equatorial F region to the
- underlying E region. Journal of Geophysical Research: Space Physics, v. 90 (A5), . 4341-4346,
- 593 doi: 10.1029/JA090iA05p04341.

594

- 595 Li, G.; Ning, B.; Wang, C.; Abdu, M. A; Otsuka, Y.; Yamamoto, M.; Wu, J.; and J. Chen (2018).
- 596 Storm-enhanced development of postsunset equatorial plasma bubbles around the meridian
- 597 120°E/60°W on 7-8 September 2017. Journal of Geophysical Research: Space Physics, v. 123 (9),
- 598 p. 7985-7998, doi: 10.1029/2018JA025871.

599

- 600 Loewe, C. A.; and G. W. Prölss (1997). Classification and mean behavior of magnetic storms.
- Journal of Geophysical Research, 102 (A7), p. 14209-14213, doi: 10.1029/96JA04020.

602

- Ma, G.; and T. Maruyama (2006). A super bubble detected by dense GPS network at east Asian
- longitudes. Geohysical Research Letters, v. 33 (21), p. 1-5, doi: 10.1029/2006GL027512.

605

- Martinis, C.; and M. Mendillo (2007). Equatorial spread F-related airglow depletions at Arecibo
- and conjugate observations. Journal of Geophysical Research: Space Physics, v. 112 (A10), p. 1-
- 608 9, doi: 10.1029/2007JA012403.

609

- Martinis, C.; Baumgardner, J.; Mendillo, M.; Coster, A.; and L. Paxton (2015). The night when the
- auroral and equatorial ionospheres converged. Journal of Geophysical Research: Space Physics, v.
- 612 120 (9), p. 8085-8095, doi: 10.1002/2015JA021555.

- Martinis, C. A.; Hickey, D.; Wroten, J.; Baumgardner, J.; Macinnis, R.; Sullivan, C.; and S. Padilla
- 615 (2020). All-sky imager observations of the latitudinal extent and zonal motion of magnetically
- 616 conjugate 630.0 nm airglow depletions. Atmosphere, v. 11(6), p. 642, doi:
- 617 10.3390/atmos11060642.

- Mendillo, M.; Zesta, E.; Shodhan, S.; Sultan, P. J.; Doe, R.; Sahai, Y.; and J. Baumgardner (2005).
- 620 Observations and modeling of the coupled latitude-altitude patterns of equatorial plasma
- depletions. Journal of Geophysical Research, v. 110 (A9303), p. 1-7, doi: 10.1029/2005JA011157.

622

- Moraes, A. O.; Sousasantos, J.; Affonso, B. J.; Silva, P. R. P.; de Paula, E. R.; and J. F. G. Monico
- 624 2023). Statistical Evaluation of the Role of GNSS Signal Propagation Orientation in Low-Latitude
- Amplitude Scintillation Severity. IEEE Open Journal of Antennas and Propagation, v. 4, p. 602-
- 626 613, doi: 10.1109/OJAP.2023.3290981.

627

- Moro, J.; Xu, J.; Denardini, C. M.; Resende, L. C. A.; Silva, R. P.; Chen, S. S.; Picanço, G. A. S.;
- Zhengkuan, L.; Li, H.; Yan, C.; Wang, C.; and N. J. Schuch (2020). Performance of the IRI-2016
- over Santa Maria, a Brazilian low-latitude station located in the central region of the South
- 631 American Magnetic Anomaly (SAMA). Annales Geophysicae, v. 38 (2), p. 457-466, doi:
- 632 10.5194/angeo-38-457-2020.

633

- Rodrigues, F. S.; and A. O. Moraes (2019). ScintPi: A low-cost, easy-to-build GPS ionospheric
- scintillation monitor for DASI studies of space weather, education, and citizen science initiatives.
- Earth and Space Science, v. 6 (8), p. 1547-1560, doi: 10.1029/2019EA000588.

637

- Rodrigues, F. S.; Socola, J. G.; Moraes, A. O.; Martinis, C.; and D. A. Hickey (2021). On the
- properties of and ionospheric conditions associated with a mid-latitude scintillation event observed
- over southern United States. Space Weather, v. 19 (6), p. 1-20, doi: 10.1029/2021SW002744.

- Senior, C.; and M. Blanc (1984). On the control of magnetospheric convection by the spatial
- distribution of ionospheric conductivities. Journal of Geophysical Research: Space Physics, v. 89
- 644 (A1), p. 261-284, doi: 10.1029/JA089iA01p00261.

- 646 Shiokawa, K.; Otsuka, Y.; Ogawa, T.; and P. Wilkinson (2004). Time evolution of high-altitude
- plasma bubbles imaged at geomagnetic conjugate points. Annales Geophysicae, v. 22 (9), p. 3137-
- 648 3143, doi: 10.5194/angeo-22-3137-2004.

649

- 650 Shiokawa, K.; Otsuka, Y.; Lynn, K. J. W.; Wilkinsn, P.; and T. Tsugawa (2015). Airglow-imaging
- observation of plasma bubble disappearance at geomagnetically conjugate points. Earth, Planets
- and Space, v. 67 (43), p. 1-12, doi: 10.1186/s40623-015-0202-6.

653

- 654 Sobral, J. H. A.; Abdu, M. A.; Pedersen, T. R.; Castilho, V. M.; Arruda, D. C. S. A.; Muella, M. T.
- A. H.; Batista, I. S.; Mascarenhas, M.; de Paula, E. R.; Kintner, P. M.; Kherai, E. A.; Medeiros, A.
- 656 F.; Buriti, R. A.; Takahashi, H.; Schuch, N. J.; Denardini, C. M.; Zamlutti, C. J.; Pimenta, A. A.;
- de Souza, J. R.; and F. C. P. Bertoni (2009). Ionospheric zonal velocities at conjugate points over
- Brazil during the COPEX campaign: Experimental observations and theoretical validations.
- 659 Journal of Geophysical Research: Space Physics, v. 114 (A4), p. 1-24, doi:
- 660 10.1029/2008JA013896.

661

- Sori, T.; Otsuka, Y.; Shinbori, A.; Nishioka, M.; and S. Perwitasari (2022). Geomagnetic conjugacy
- of plasma bubbles extending to mid-latitudes during a geomagnetic storm on March 1, 2013. Eath,
- Planets and Space, v. 74 (120), p. 1-16, doi: 10.1186/s40623-022-01682-7.

665

- Sousasantos, J.; Abdu, M. A.; de Paula, E R.; Moraes, A. O.; Salles, L. A.; and B. J. Affonso
- 667 (2022a). Conjugated asymmetry of the onset and magnitude of GPS scintillation driven by the
- vertical plasma drift. GPS Solutions, v. 26 (75), p. 1-13, doi: 10.1007/s10291-022-01258-8.

669

- 670 Sousasantos, J.; Affonso, B. J.; Moraes, A. O.; Rodrigues, A. O.; Abdu, M. A.; Salles, L. A.; and
- B. C. Vani (2022b). Amplitude scintillation severity and fading profiles under alignment between
- 672 GPS propagation paths and equatorial plasma bubbles. Space Weather, v. 20 (11), p. 1-15, doi:
- 673 10.1029/2022SW003243.

- 675 Sousasantos, J.; Gomez Socola, J.; Rodrigues, F. S.; Eastes, R. W.; Brum, C. G. M.; and P. Terra
- 676 (2023). Severe L-band scintillation over low-to-mid latitudes caused by an extreme equatorial
- plasma bubble: joint observations from ground-based monitors and GOLD. Earth, Planets and
- 678 Space, v. 75 (41), p. 1-12, doi: 10.1186/s40623-023-01797-5.

- 680 Sousasantos, J.; Rodrigues, F. S.; Moraes, A. O.; Eastes, R. W.; and J. F. G. Monico (2024a). On
- the estimation of scintillation severity using background F-region peak densities: description and
- example results using GOLD observations. GPS Solutions, v. 28 (2), p. 1-11, doi: 10.1007/s10291-
- 683 023-01602-6.

684

- Sousasantos, J.; Rodrigues, F. S.; Gomez Socola, J.; Pérez, C.; Colvero, F.; Martinis, C. R.; and C.
- 686 M. Wrasse (2024b). First observations of severe scintillation over low-to-mid latitudes driven by
- quiet-time extreme equatorial plasma bubbles: conjugate measurements enabled by citizen science
- 688 initiatives [Dataset]. Zenodo. https://doi.org/10.5281/zenodo.11086858.

689

- 690 Souza, J. R.; Bailey, G. J.; Abdu, M. A.; and I. S. Batista (2000). Ionospheric modelling at low
- latitudes over Brazil during summer solar minimum. Advances in Space Research, v. 25 (1), p.
- 692 133-138, doi: 10.1016/S0273-1177(99)00910-2.

693

- 694 Spogli, L.; Alfonsi, L.; Romano, V.; De Franceschi, G.; Monico, J. F. G.; Shimabukuro, M. H.;
- Bougard, B.; and M. Aquino (2013). Assessing the GNSS scintillation climate over Brazil under
- 696 increasing solar activity. Journal of Atmospheric and Solar-Terrestrial Physics, v. 105-106, p. 199-
- 697 206, doi: 10.1016/j.jastp.2013.10.003.

698

- 699 Spreiter, J. R.; and B. R. Briggs (1961). Theory of electrostatic fields in the ionosphere at equatorial
- 700 latitudes. Journal of Geophysical Research, v. 66(8), p. 2345-2354, doi:
- 701 10.1029/JZ066i008p02345.

- Sreeja, V. V.; Aquino, M.; Marques, H. A.; and A. O. Moraes (2020). Mitigation of ionospheric
- scintillation effects on GNSS precise point positioning (PPP) at low latitudes. Journal of Geodesy,
- 705 v. 94 (15), p. 1-10, doi: 10.1007/s00190-020-01345-z.

- 706
- Vani, B. C.; Moraes, A. O.; Salles, L. A., Breder, V. H. F., dos Santos Freitas, M. J.; Monico, J. F.
- 708 G.; and de Paula, E. R. (2021). Monitoring ionospheric scintillations with GNSS in South America:
- 709 Scope, results, and challenges. In GPS and GNSS Technology in Geosciences, Elsevier, p. 255-
- 710 280, doi: 10.1016/B978-0-12-818617-6.00012-3.
- 711
- Wright, I. G.; Solanki, I.; Desai, A.; Gomez Socola, J.; and F. S. Rodrigues (2023). Student-led
- design, development and tests of an autonomous, low-cost platform for distributed space weather
- observations. Journal of Space Weather and Space Climate, v. 13(12), p. 1-11, doi: 10.1051/
- 715 swsc/2023010.
- 716
- Yeh, K. C.; and C. H. Liu (1982). Radio wave scintillations in the ionosphere. Proceedings of the
- 718 IEEE, v. 70 (4), p. 324-360, doi: 10.1109/PROC.1982.12313.
- 719
- 720 Zakharenkova, I.; and I. Cherniak (2020). When plasma streams tie up equatorial plasma
- 721 irregularities with auroral ones. Space Weather, v. 18 (2), p. 1-19, doi: 10.1029/2019SW002375.
- 722
- 723 Zakharenkova, I.; and I. Cherniak (2021). Effects of storm-induced equatorial plasma bubbles on
- 724 GPS-based kinematic positioning at equatorial and middle latitudes during the September 7–8,
- 725 2017, geomagnetic storm. GPS Solutions, v. 25 (132), p. 1-14, doi: 10.1007/s10291-021-01166-3.